

RESEARCH

Open Access



Development and validation of a machine learning-derived radiomics model for diagnosis of osteoporosis and osteopenia using quantitative computed tomography

Qianrong Xie^{1,2†}, Yue Chen^{3†}, Yimei Hu^{4†}, Fanwei Zeng¹, Pingxi Wang⁵, Lin Xu⁶, Jianhong Wu⁵, Jie Li¹, Jing Zhu^{7*}, Ming Xiang^{3,8*} and Fanxin Zeng^{1,3*}

Abstract

Background: To develop and validate a quantitative computed tomography (QCT) based radiomics model for discriminating osteoporosis and osteopenia.

Methods: A total of 635 patients underwent QCT were retrospectively included from November 2016 to November 2019. The patients with osteopenia or osteoporosis (N = 590) were divided into a training cohort (N = 414) and a test cohort (N = 176). Radiomics features were extracted from the QCT images of the third lumbar vertebra. Minimum redundancy and maximum relevance and least absolute shrinkage and selection operator were used for data dimensional reduction, features selection and radiomics model building. Multivariable logistic regression was applied to construct the combined clinical-radiomic model that incorporated radiomics signatures and clinical characteristics. The performance of the combined clinical-radiomic model was evaluated by the area under the curve of receiver operator characteristic curve (ROC–AUC), accuracy, specificity, sensitivity, positive predictive value, and negative predictive value.

Results: The patients with osteopenia or osteoporosis were randomly divided into training and test cohort with a ratio of 7:3. Six more predictive radiomics signatures, age, alkaline phosphatase and homocysteine were selected to construct the combined clinical-radiomic model for diagnosis of osteoporosis and osteopenia. The AUC of the combined clinical-radiomic model was 0.96 (95% confidence interval (CI), 0.95 to 0.98) in the training cohort and 0.96 (95% CI 0.92 to 1.00) in the test cohort, which were superior to the clinical model alone (training-AUC = 0.81,

[†]Qianrong Xie, Yue Chen and Yimei Hu These authors contribute equally.

*Correspondence: zhujingys@sina.com; josceph_xm@sina.com; zengfx@pku.edu.cn

¹ Department of Clinical Research Center, Dazhou Central Hospital, No.56 Nanyuemiao Street, Tongchuan District, Dazhou 635000, Sichuan, China

³ Department of Clinical Medicine, Chengdu University of Traditional Chinese Medicine, No. 37 Shi-er-qiao Road, Jinniu District, Chengdu 610000, Sichuan, China

⁷ Department of Rheumatology and Immunology, Sichuan Academy of Medical Sciences and Sichuan Provincial People's Hospital, No.32 First Ring Road West, Jinniu District, Chengdu 610000, Sichuan, China

Full list of author information is available at the end of the article



test-AUC = 0.79). The calibration curve demonstrated that the radiomics nomogram had good agreement between prediction and observation and decision curve analysis confirmed clinically useful.

Conclusions: The combined clinical-radiomic model that incorporates the radiomics score and clinical risk factors, can serve as a reliable and powerful tool for discriminating osteoporosis and osteopenia.

Keywords: Combined clinical-radiomic model, Osteoporosis, Osteopenia, Quantitative computed tomography

Introduction

Osteoporosis is a age-related musculoskeletal disease characterized by reduced bone mass and increasing of bone fragility and fracture susceptibility [1]. Obviously, aging of population is becoming more severe and it has been estimated about 6 million fragility fractures will occur in China by 2050 [2]. Early screening and intervention will effectively slow down the development of bone resorption and reduce the risk for initial or subsequent fractures [3].

Dual energy X-ray (DXA) is currently widely used for diagnosis of osteoporosis, but it may be interfered by vascular calcification, osteophyte, and body position. Quantitative computed tomography (QCT) is also an imaging technique based on radiation absorption to measure volumetric density, which can assess cortical and trabecular bone compartments separately [4]. The changes of bone mineral density (BMD) measured by QCT are more sensitive to age-related or treatment-related than that measured by DXA for the whole vertebral body [4].

Since radiomics [5–9] was proposed in 2012, a high-throughput approach of mining-specific image characteristics from standard medical images, which has drawn increasing attentions. It extracts a large number of

features and applies them to the clinical decision support systems to improve the accuracy of qualitative evaluation and prognosis of lesions. Radiomics has been successfully applied in prediction and differentiation of disease outcome in high-risk prostate cancer [10], bone mineral loss [11], osteopenia and osteoporosis for X-ray [12], osteoporosis prediction [13] and types of multiple myeloma [5]. Tagliafico AS et al. [5] was the first study bringing radiomics signatures into musculoskeletal system to differentiate bone tissue into focal and diffuse pattern of multiple myeloma, and their model validation effective rates were 73–71%, respectively.

Therefore, our study aimed to establish and validate a nomogram radiomics model that incorporated both the radiomics signatures based on QCT images and clinic risk factors to evaluate osteoporosis and osteopenia for individual pre-treatment.

Methods

Patients

The participants were included from Dazhou Central Hospital between November 2016 and November 2019. 1120 cases who received QCT were retrospectively collected (Fig. 1). The exclusion criteria were as followed: i.

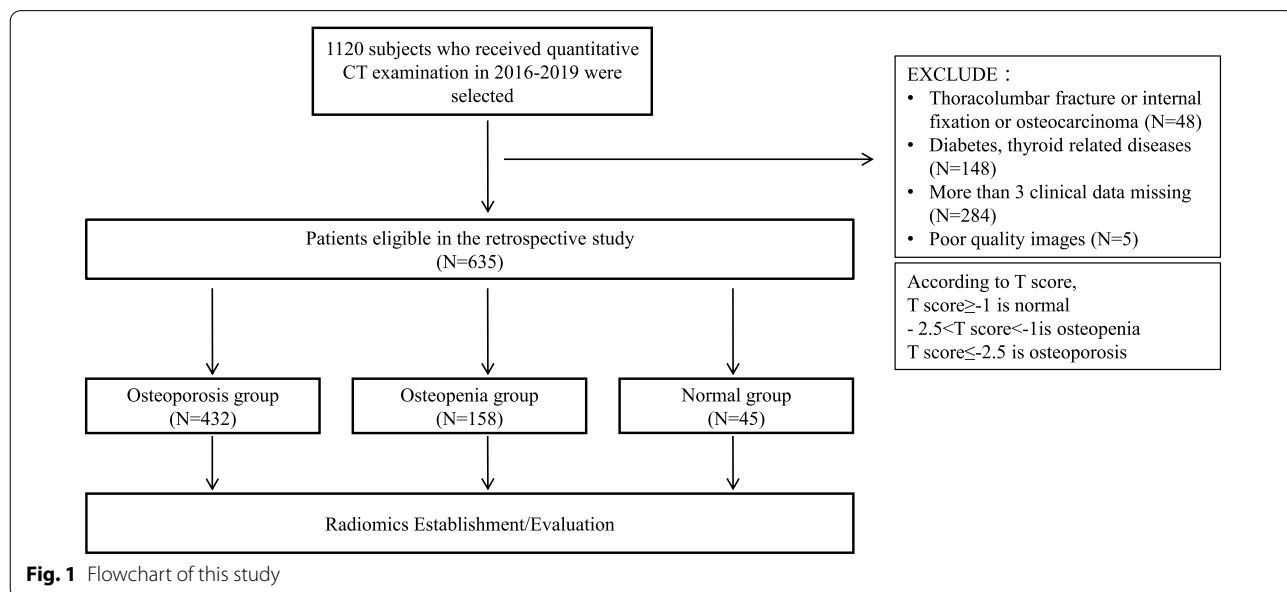


Fig. 1 Flowchart of this study

lumbar fracture or lumbar fracture with internal fixation; ii. malignant space occupying lesions of lumbar vertebra; iii. metabolic or endocrine diseases such as hyperthyroidism or hypothyroidism, occupying lesions of thyroid, diabetes, neurological diseases (such as parkinson's disease and alzheimer's disease); iv. chronic obstructive pulmonary disease; v. poor quality images; vi. more than 3 items of clinical characteristics were missed. Gender, age, hemoglobin (Hb), glucose, total bilirubin, direct bilirubin, indirect bilirubin, alkaline phosphatase (ALP), uric acid (UA), calcium (Ca), magnesium (Mg), phosphorus (P), homocysteine (Hcy) and other clinical information in the same period were collected from the medical records of patients. The patients were classified into normal ($T\text{-score} \geq -1$), osteopenia ($-2.5 < T\text{-score} < -1$) and osteoporosis ($T\text{-score} \leq -2.5$) groups according to the T-score. The T-score was calculated from bone mineral density. The calculation formula is: $Db = (Hb - Hw) / (Hk - Hw) \times Ck$, $T\text{-score} = (BMD_{(Patients)} - BMD_{(Healthy\ young\ people)}) / SD_{(Control)}$, which Db was the BMD, Hb was the CT value of ROI, Hk was the CT value of phantom, Hw was the CT value of water, and the Ck was the density of phantom. The study was approved by the ethics committee of Dazhou Central Hospital and kept with the policies for a retrospective review, informed consent was not required.

Region of interest (ROI) segmentation and feature extraction

The images were acquired using SOMATOM Definition AS (Siemens Healthcare, Forchheim, Germany). The QCT scan parameters were 80 kV tube voltage, 10 mm slice width, 1 s exam time. The T-score were obtained by analyzing QCT images with osteo software (Siemens Healthcare, Forchheim, Germany). The image parameters were as follows: acquisition matrix = 512×512 . The CT images were retrieved from the INFINITT Picture Archiving and Communication Systems (PACS) (INFINITT Healthcare, Seoul, Korea) and then exported to the 3D slicer software (version 4.10.2; www.slicer.org) (USA National Institutes of health, Bethesda, USA) for manual segmentation. In this study, all the images were Digital Imaging and Communications in Medicine (DICOM) format. The ROI were manually segmented by two medical students under the guidance of experienced radiologists. Pyradiomics installed in 3D slicer was used to extract feature [14] and the wavelet filters was applied in the feature extraction steps, which is compliant with Image Biomarker Standardization Initiative (IBSI) [15]. We did not perform voxel resampling. The initial setting used for the feature extraction process was showed in Additional file 1: Table S1. The cancellous bone of the third lumbar vertebrae (L3) were segmented and

851 quantitative features were produced. These features included shape, gray level dependence matrix (gldm), gray-level co-occurrence matrix (glcm), firstorder, gray-level run-length matrix (glrlm), gray-level size zone matrix (glszm), neighborhood gray-tone difference matrix (ngtdm).

Inter- and Intra-observer Reproducibility Evaluation

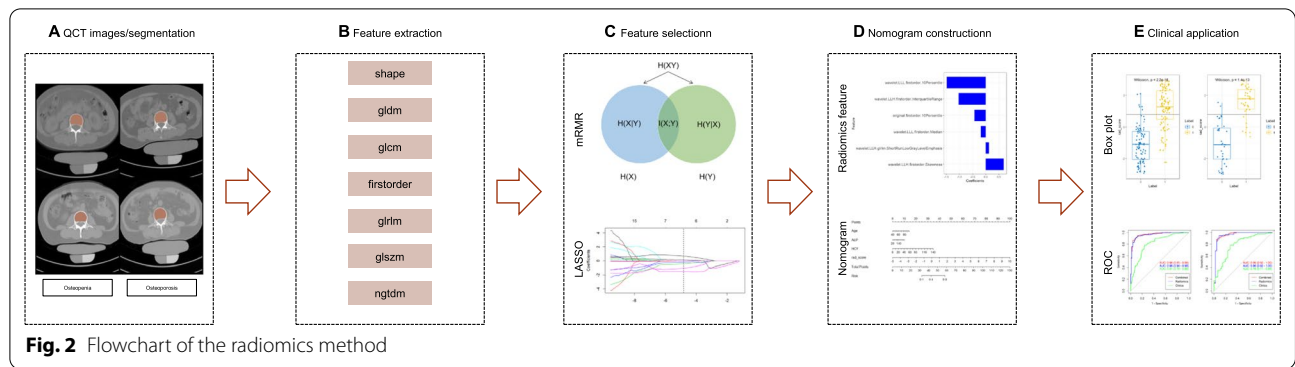
Twenty consecutive patient images were selected for inter- and intra- observer reproducibility comparison. Each observer repeated the generation 851 of radiomic features twice within a half year period following the same procedure to assess intra-observer reproducibility.

Radiomics nomogram construction

Eligible patients were randomly allocated to training and test cohorts in a ratio of 7:3. The "preProcess" function in R was used for feature standardization (centering and scaling). Minimum redundancy and maximum relevance (mRMR) [16] was used to pre-selected 851 radiomics signatures, then the least absolute shrinkage and selection operator (LASSO) was further selected the remained features to reduce redundancy. The mRMR utilizes the information entropy and difference to select features, so that the selected features have the minimum redundancy and meet the maximum correlation. LASSO regression model excludes the secondary independent variable coefficient by regression penalty. Multiple logistic regression model was used to select candidate factors of clinical information, such as age, gender, and other biochemistry metrics. An overview of the combined model process was shown in the Fig. 2.

Statistical analysis

Statistical analysis was performed using SPSS 20.0 (International Business Machines Corporation, State of New York, USA) and R software (version 3.6.1) (R studio, Boston, USA). The "mRMRe" and "glmnet" packages in R were used to build mRMR and LASSO. The nomogram was built using "rms" package. The independent sample *t*-test or Mann-Whitney *U* test was used to analyze the relationship between quantitative data (Age, HGB, GLU, TBIL, DBIL, IBIL, ALP, UA, Ca, Mg, P, HCY), but the Chi-square test was used to analyze the categorical data (Gender). The area under the curve (AUC), accuracy, specificity, sensitivity, positive predictive value and negative predictive value were used to evaluate the performance of the model for distinguishing the osteoporosis and osteopenia. In order to assess the difference of receive operating characteristic, the Delong's test was used. The calibration curves accompanied by Hosmer-Lemeshow *H* test were used to evaluate whether the model was perfectly calibrated. Intra-class correlation



coefficients (ICCs) was used to evaluate the inter- and intra- observer reproducibility based on the extracted features, which 0.81–1.00 was considered to be perfect agreement. Two-tailed $P < 0.05$ was considered to have significant difference.

Results

Patients

A total of 635 patients were eligible for inclusion in our study (Fig. 1). We divided patients into a training cohort ($N = 414$) and a test cohort ($N = 176$). The characteristics of patients were presented in Table 1 and Additional file 1: Table S1. Age, ALP and Hcy were the top three

different clinical characteristics between osteoporosis and osteopenia in the training group ($P < 0.05$).

Feature selection and radiomics score (rad-score) construction

Supporting Information (ICCs of intra- and inter-observer was perfect agreement.)

A combined mRMR and LASSO methodological approach was used to select the 6 optimal radiomics features. Firstly, there were 20 potential predictors from 851 features selected by the mRMR (Additional file 1: Fig. S1A). Then, the LASSO was further selected 6 optimal features with nonzero coefficients (Additional

Table 1 Characteristics of Patients in the Training and Test Cohorts

| Characteristics | Training cohorts | | | Test cohorts | | P |
|-------------------------|------------------|---------------|---------|---------------|----------------|---------|
| | Osteoporosis | Osteopenia | P | Osteoporosis | Osteopenia | |
| Gender, No. (%) | | | 0.032* | | | 0.897 |
| Male | 86 (28.40) | 20 (18.00) | | 29 (22.50) | 11 (23.40) | |
| Female | 217 (71.60) | 91 (82.00) | | 100 (77.50) | 36 (76.60) | |
| Age, mean (SE), years | 70.03 (0.55) | 58.32 (0.92) | <0.001* | 69.11 (0.85) | 57.72 (1.45) | <0.001* |
| HGB, mean (SE), g/L | 122.28 (1.67) | 127.83 (1.59) | 0.209 | 125.46 (1.54) | 127.17 (2.60) | 0.385 |
| GLU, mean (SE), mmol/L | 5.56 (0.07) | 5.21 (0.13) | 0.010* | 5.80 (0.15) | 5.28 (0.08) | 0.010* |
| TBIL, mean (SE), umol/L | 17.18 (3.83) | 13.02 (0.59) | 0.354 | 14.52 (0.69) | 14.86 (0.89) | 0.341 |
| DBIL, mean (SE), umol/L | 4.66 (0.91) | 3.11 (0.13) | 0.001 | 4.30 (0.35) | 3.74 (0.34) | 0.435 |
| IBIL, mean (SE), umol/L | 13.56 (3.95) | 9.91 (0.49) | 0.935 | 10.22 (0.45) | 11.17 (0.70) | 0.115 |
| ALP, mean (SE), U/L | 84.49 (1.50) | 76.13 (2.40) | 0.001* | 85.06 (3.36) | 75.84 (3.64) | 0.153 |
| UA, mean (SE), umol/L | 301.77 (4.69) | 305.54 (8.48) | 0.851 | 307.97 (8.39) | 296.66 (10.19) | 0.351 |
| Ca, mean (SE), mmol/L | 2.64 (0.34) | 2.34 (0.01) | 0.001 | 2.29 (0.01) | 2.33 (0.02) | 0.049* |
| Mg, mean (SE), mmol/L | 1.06 (0.01) | 1.04 (0.02) | 0.968 | 1.07 (0.02) | 1.01 (0.02) | 0.062 |
| P, mean (SE), mmol/L | 1.09 (0.01) | 1.13 (0.02) | 0.047* | 1.09 (0.01) | 1.10 (0.02) | 0.858 |
| Hcy, mean (SE), umol/L | 14.83 (0.58) | 11.48 (0.50) | <0.001* | 14.90 (0.86) | 12.83 (0.71) | 0.252 |

P value is derived from the univariable association analyses. Chi-Square was used to analyze the difference of categorical data (Gender), while the independent sample t-test or Mann–Whitney U test was used to analyze the difference of quantitative data (Age, HGB, GLU, TBIL, DBIL, IBIL, ALP, UA, Ca, Mg, P, HCY)

HGB hemoglobin, GLU glucose, TBIL total bilirubin, DBIL direct bilirubin, IBIL indirect bilirubin, ALP alkaline phosphatase, UA uric acid, Ca calcium, Mg magnesium, P phosphorus, HCY homocysteine, SE standard error

* P value < 0.05

file 1: Fig. S1B, C). The features included wavelet_LLL_firstorder_10Percentile, wavelet_LLH_firstorder_InterquartileRange, original_firstorder_10Percentile, wavelet_LLL_firstorder_Median, wavelet_LLH_glrml_ShortRunLowGrayLevelEmphasis, wavelet_LLH_firstorder_Skewness. The contribution of the selected features was shown in Additional file 1: Fig. S2 and the rad-score were shown in supplementary materials. The rad-score showed the excellent diagnosis performance in discriminating the osteoporosis and osteopenia in training ($P < 0.001$) and test cohort ($P < 0.001$) (Additional file 1: Fig. S3).

Development and validation of a radiomics model

We constructed two models to distinguishing osteoporosis and osteopenia based on the radiomics features or clinical variables, respectively. The AUC of the radiomics model was 0.96 (95% confidence interval (CI), 0.94–0.98) in the training cohort and 0.96 (95% CI 0.92–1.00) in the test cohort (Fig. 3). The clinical model yielded an

AUC of 0.81 (95% CI 0.78–0.86) in the training cohort and 0.79 (95% CI 0.71–0.86) in the test cohort. Furthermore, the model combined with the clinical variables and radiomics features of AUC was 0.96 (95% CI 0.95–0.98) in the training cohort, while the AUC was 0.96 (95% CI 0.92–1.00) in the test cohort. The results showed that the radiomics model was not inferior to the combined clinical-radiomic model both in the training and test cohort (Fig. 3). In addition, we compared the diagnostic performance among the clinics, radiomics and combined model using accuracy, sensitivity, specificity both in the training and test group (Table 2). A nomogram was conducted based on the rad-score and 3 clinical characteristics (Age, ALP, Hcy) for differentiation of osteoporosis and osteopenia (Fig. 4A). The calibration curve showed good agreement between prediction and observation in both cohort (Fig. 4B, C). The P -value (0.95 in the training cohort and 0.09 in the test cohort) using the Hosmer–Lemeshow H test showed had no departure from the perfect fit. Furthermore, we

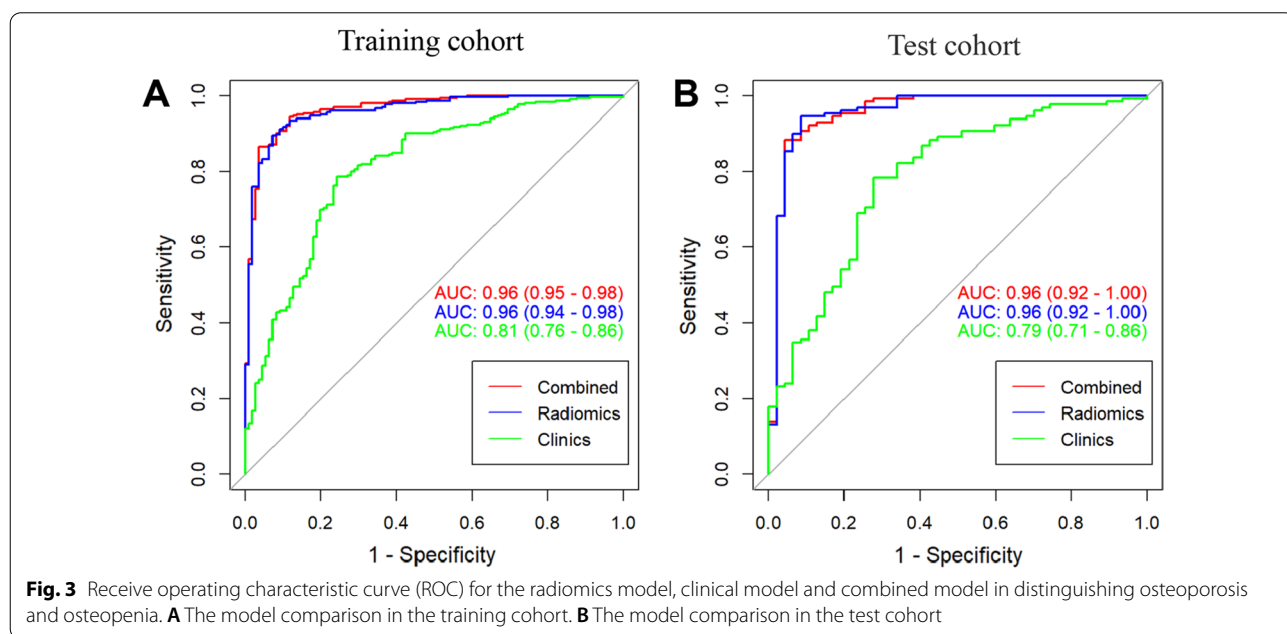
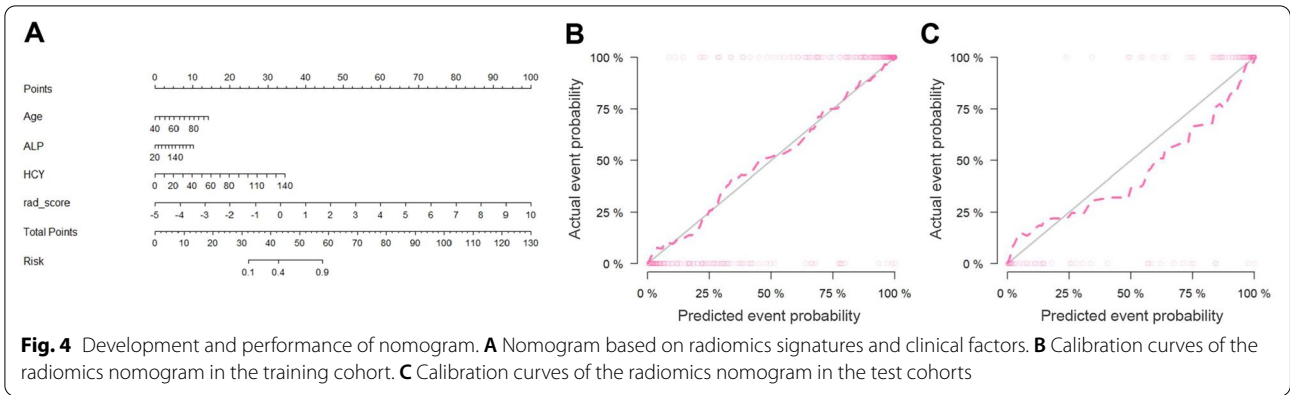


Fig. 3 Receive operating characteristic curve (ROC) for the radiomics model, clinical model and combined model in distinguishing osteoporosis and osteopenia. **A** The model comparison in the training cohort. **B** The model comparison in the test cohort

Table 2 Diagnostic performance of clinical, radiomics and combined clinical-radiomic model

| Group | Model | Accuracy | Sensitivity | Specificity | PPV | NPV |
|----------|-----------------------------|----------|-------------|-------------|------|------|
| Training | Clinics | 0.78 | 0.90 | 0.56 | 0.79 | 0.76 |
| Test | Clinics | 0.74 | 0.88 | 0.51 | 0.74 | 0.72 |
| Training | Radiomics | 0.90 | 0.93 | 0.89 | 0.76 | 0.97 |
| Test | Radiomics | 0.94 | 0.92 | 0.95 | 0.86 | 0.97 |
| Training | Combined clinical-radiomics | 0.89 | 0.99 | 0.72 | 0.87 | 0.96 |
| Test | Combined clinical-radiomics | 0.90 | 0.98 | 0.75 | 0.88 | 0.96 |

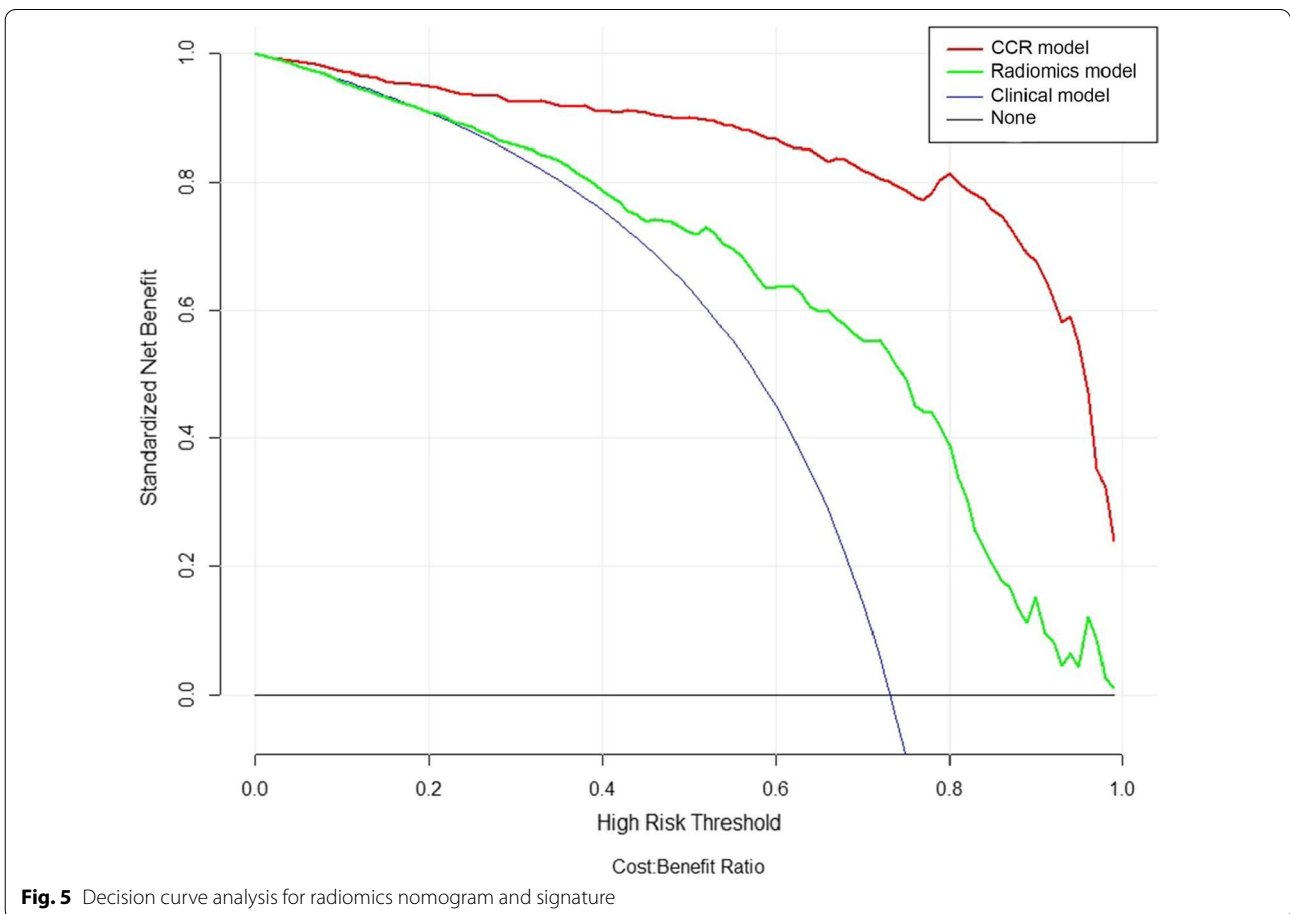
PPV positive predictive value, NPV negative predictive value



compared the normal and patients with bone loss to validate the performance of the rad-score in different subgroups. The results were considerably good especially in differentiating osteoporosis and normal subjects (AUC = 0.99, 95% CI 0.98–1.00), and the AUC of bone loss patients and normal subjects was 0.90 (95% CI 0.87–0.93), the AUC of osteopenia and normal was 0.66 (95% CI 0.57–0.75) (Additional file 1: Fig. S4).

Clinical use

The decision curve of the radiomics, clinical and combined clinical-radiomic model was shown in Fig. 5. The nomogram with rad-score was considered better than clinical model in discriminating the osteoporosis and osteopenia when the threshold probability in the early stage. The net benefit of combined clinical-radiomic model was higher than clinical model in all the range.



Discussion

This study built and validated a diagnostic model of bone mass individualization based on QCT images, with a large sample that successfully distinguished the osteoporosis and osteopenia patients. We found that the radiomics features can supplement the current clinical diagnostic system, and it provides a better discrimination and evaluation ability for the development of bone loss meanwhile.

BMD is the most important parameter in the diagnosis of osteoporosis. However, it can not reflect the bone microstructure. In comparison to BMD obtained by QCT, bone microstructure parameters brings additional and complementary information to improve the prediction of fracture risk [17, 18]. As a new technology, radiomics can produce many features that reflect the microstructure of images. Some studies have shown that there is a certain correlation between the texture parameters of cancellous bone extracted from radiological images and bone microstructure [19, 20]. He et al. have established a radiomics model based on MRI for the diagnosis of osteoporosis [21]. In our study, the model based on QCT images and clinical data can quantify the information of higher dimensions of vertebral body to a certain extent, which is comprehensively analyze the changes of bone structure and bone mineral density, and has certain application value for the evaluation of osteoporosis.

For the construction of the radiomics signatures, 851 candidate radiomics features were shrunk to 20 potential predictors with mRMR feature selection to eliminate the redundant and irrelevant features. Then, LASSO approach was used to reduce the regression coefficient, extract 6 features with high performance of discrimination for osteoporosis and osteopenia to establish rad-score. Signatures extracted from LASSO were considerable accurately and the regression coefficients of most signatures were reduced toward zero during overfitting [22], making the model easier to construe and available to identify the top ranking signatures [23]. Compared to the clinical predictors alone (training-AUC=0.81, test-AUC=0.79), the combined model showed significant improvement (AUC=0.96).

We used QCT images to extract the meaningful radiomics features in discriminating bone density changes and osteoporosis and received a considerable performance (AUC=0.96). Previous model [24] based on DXA images investigate the diagnostic accuracy of bone mass classification using several machine learning algorithms, showing a small sample capacity and a lower AUC that ranging between 0.50 and 0.78. Lee KS et al. explored the reliability the reliability of using dental tablets to screen osteoporosis (AUC=0.858) [25]. Several studies

has confirmed that [26–28] the lumbar spine is the good observation site for bone loss in all skeletal structures, among long bone backbone, femoral neck, and spinal segment [29, 30]. Among the lumbar vertebrae, the L3 has the highest specificity [26], because L3 is found to be the vertebral body with the highest bone metabolism rate and the lowest bone density in all vertebral bodies. In our study, the L3 was used to extract radiomics signatures, and it was proved that the extracted signatures could significantly discriminate the osteoporosis and osteopenia (AUC=0.96). In comparison, some studies developed a predictive model for BMD based on hip BMD [31], lumbar and hip BMD [32] or unspecified [33]. The delineation of ROI is the most important part in the analysis of radiomics, because the subsequent data is generated by the delineated area, and the gray scale of cancellous bone and cortical bone is clear and easy to distinguish.

The 6 more predictive radiomics signatures mainly concluded wavelet_LLH features, which had been proved having high discriminating and predictable performance of model verification, especially in distant metastases of lung cancer [34] and improvement of radiomics reproducibility for pulmonary nodules or masses [35]. In these 6 features, 2 were the wavelet_LLL features, 3 were wavelet_LLH features and 1 was original feature. In addition, features include both first-order features and grayscale features. Wavelet features could reflect the spatial heterogeneity of vertebral body synthetically cause they contain high-order image [36]. Studies have shown that both skewness and glrlm can reflect the heterogeneity of regions of interest [37–39]. Our analysis demonstrated that the 6 radiomics features had a strong discrimination ability to evaluate osteoporosis and osteopenia. Previous studies [40–42] proposed that age, gender, Hb, UA, Hcy, ALP, Ca, are related with osteoporosis, but the correlations are weakly positive compared to BMD [40]. In our study, the specific clinical predictors performed a training AUC of 0.81 and a test AUC of 0.79. Therefore, our results showed that adding the rad-score to the model can improve the performance of clinical nomogram (training-AUC=0.96, test-AUC=0.96). This finding may support multi-dimension data is most effectively way to construct clinical decision model. However, some studies only use clinical data to diagnose osteoporosis [43, 44]. There are several limitations in our study. First, this study was derived from single center and there is no external data, so its performance evaluation may be overly optimistic. Second, the follow-up data like therapeutic response and fracture rate was not considered currently.

In summary, a rad-score derived from QCT images was proposed in this study, which was an independent risk factor for abnormal BMD patients. In addition, diagnostic nomograms combining rad-score and clinical predictors

provided a convenient way to discriminate osteoporosis and osteopenia and may influence decision-making on the possible benefit of treatment.

Supplementary Information

The online version contains supplementary material available at <https://doi.org/10.1186/s12880-022-00868-5>.

Additional file 1: Figure S1. Radiomics feature selection using minimum redundancy and maximum relevance (mRMR) and least absolute shrinkage and selection operator (LASSO). **Figure S2.** The contribution of each feature to the radiomic signature was shown by histogram. **Figure S3.** Performance of rad-score in discriminating between osteoporosis and osteopenia. **Figure S4.** Performance of rad-score in discriminating between normal and osteopenia, abnormal and osteoporosis. **Table S1.** Pyradiomics plug-in unit extraction parameters (v2.2). **Table S2.** Characteristics of Patients.

Acknowledgements

We would like to thank all study patients and their families for their cooperation and contributions of tissue for analysis.

Author contributions

QX, YC, YH drafted the manuscript and collected the data. YH and FZ revised the manuscript. PW, LX, JW and JL were involved the clinical problems interpretation of this study. JZ and MX revised the manuscript. FZ designed this work and analyzed the data. All authors approved the final manuscript and agreed to be accountable for all aspects of the work.

Funding

This study was funded by the National Natural Science Foundation of China (81902861), Sichuan Medical Association (S20001, S19062), Department of Science and Technology of Sichuan Province (2021YFS0165, 22ZDYF1942, 22ZDYF1766).

Availability of data and materials

The datasets used and/or analysed during the current study are available from the corresponding author on reasonable request.

Declarations

Ethics approval and consent to participate

The study was approved by the ethics committee of Dazhou Central Hospital. The committee of Dazhou Central Hospital waived the need for patients to sign informed consent. All methods were carried out in accordance with relevant guidelines and regulations.

Consent for publication

Not applicable.

Competing interests

The authors declare that they have no conflict of interest.

Author details

¹Department of Clinical Research Center, Dazhou Central Hospital, No.56 Nanyuemiao Street, Tongchuan District, Dazhou 635000, Sichuan, China. ²Department of Laboratory Medicine, The Third People's Hospital of Chengdu, Chengdu 610000, China. ³Department of Clinical Medicine, Chengdu University of Traditional Chinese Medicine, No. 37 Shi-er-qiao Road, Jinniu District, Chengdu 610000, Sichuan, China. ⁴Department of Orthopedics, Hospital of Chengdu University of Traditional Chinese Medicine, Chengdu 610000, China. ⁵Department of Bone Disease, Dazhou Central Hospital, Dazhou 635000, China. ⁶Department of Medical Imaging, Dazhou Central Hospital, Dazhou 635000, China. ⁷Department of Rheumatology and Immunology, Sichuan Academy of Medical Sciences and Sichuan Provincial People's Hospital, No.32 First Ring Road West, Jinniu District, Chengdu 610000, Sichuan,

China. ⁸Department of Orthopedics, Sichuan Provincial Orthopedic Hospital, Chengdu 610000, China.

Received: 31 March 2022 Accepted: 26 July 2022

Published online: 08 August 2022

References

- Consensus development conference. diagnosis, prophylaxis, and treatment of osteoporosis. *Am J Med.* 1993;94(6):646–50.
- Si L, Winzenberg TM, Jiang Q, Chen M, Palmer AJ. Projection of osteoporosis-related fractures and costs in China: 2010–2050. *Osteoporos Int.* 2015;26(7):1929–37.
- Qaseem A, Forciea MA, McLean RM, Denberg TD. Clinical guidelines committee of the American college of P. Treatment of low bone density or osteoporosis to prevent fractures in men and women: a clinical practice guideline update from the American college of physicians. *Ann Intern Med.* 2017;166(11):818–39.
- Engelke K, Adams JE, Armbrrecht G, Augat P, Bogado CE, Bouxsein ML, et al. Clinical use of quantitative computed tomography and peripheral quantitative computed tomography in the management of osteoporosis in adults: the 2007 ISCD official positions. *J Clin Densitom.* 2008;11(1):123–62.
- Tagliafico AS, Cea M, Rossi F, Valdora F, Bignotti B, Succio G, et al. Differentiating diffuse from focal pattern on computed tomography in multiple myeloma: added value of a radiomics approach. *Eur J Radiol.* 2019;121:108739.
- Zhang B, Tian J, Dong D, Gu D, Dong Y, Zhang L, et al. Radiomics features of multiparametric MRI as novel prognostic factors in advanced nasopharyngeal carcinoma. *Clin Cancer Res.* 2017;23(15):4259–69.
- Dong D, Tang L, Li ZY, Fang MJ, Gao JB, Shan XH, et al. Development and validation of an individualized nomogram to identify occult peritoneal metastasis in patients with advanced gastric cancer. *Ann Oncol.* 2019;30(3):431–8.
- Lambin P, Rios-Velazquez E, Leijenaar R, Carvalho S, van Stiphout RG, Granton P, et al. Radiomics: extracting more information from medical images using advanced feature analysis. *Eur J Cancer.* 2012;48(4):441–6.
- Ibrahim A, Primakov S, Beuque M, Woodruff HC, Halilaj I, Wu G, et al. Radiomics for precision medicine: current challenges, future prospects, and the proposal of a new framework. *Methods.* 2021;188:20–9.
- Alongi P, Stefano A, Comelli A, Laudicella R, Scalisi S, Arnone G, et al. Radiomics analysis of 18F-Choline PET/CT in the prediction of disease outcome in high-risk prostate cancer: an explorative study on machine learning feature classification in 94 patients. *Eur Radiol.* 2021;31(7):4595–605.
- Rastegar S, Vaziri M, Qasempour Y, Akhsh MR, Abdalvand N, Shiri I, et al. Radiomics for classification of bone mineral loss: a machine learning study. *Diagn Interv Imaging.* 2020;101(9):599–610.
- Zhang B, Yu K, Ning Z, Wang K, Dong Y, Liu X, et al. Deep learning of lumbar spine X-ray for osteopenia and osteoporosis screening: a multicenter retrospective cohort study. *Bone.* 2020;140: 115561.
- Stephanakis, Ioannis, M., Anagnostopoulos, Christos-Nikolaos, Iliou, et al. A novel data preprocessing method for boosting neural network performance: A case study in osteoporosis prediction. *Information Sciences: An International Journal.* 2017;380:92–100.
- van Griethuysen JJM, Fedorov A, Parmar C, Hosny A, Aucoin N, Narayan V, et al. Computational radiomics system to decode the radiographic phenotype. *Cancer Res.* 2017;77(21):e104–7.
- Fornacon-Wood I, Mistry H, Ackermann CJ, Blackhall F, McPartlin A, Faivre-Finn C, et al. Reliability and prognostic value of radiomic features are highly dependent on choice of feature extraction platform. *Eur Radiol.* 2020;30(11):6241–50.
- Peng H, Long F, Ding C. Feature selection based on mutual information: criteria of max-dependency, max-relevance, and min-redundancy. *IEEE Trans Pattern Anal Mach Intell.* 2005;27(8):1226–38.
- Baum T, Karampinos DC, Liebl H, Rummeny EJ, Waldt S, Bauer JS. High-resolution bone imaging for osteoporosis diagnostics and therapy monitoring using clinical MDCT and MRI. *Curr Med Chem.* 2013;20(38):4844–52.

18. Link TM. Osteoporosis imaging: state of the art and advanced imaging. *Radiology*. 2012;263(1):3–17.
19. Jeong H, Kim J, Ishida T, Akiyama M, Kim Y. Computerised analysis of osteoporotic bone patterns using texture parameters characterising bone architecture. *Br J Radiol*. 2013;86(1021):20101115.
20. Baum T, Grabeldinger M, Rath C, Garcia EG, Burgkart R, Patsch JM, et al. Trabecular bone structure analysis of the spine using clinical MDCT: can it predict vertebral bone strength? *J Bone Miner Metab*. 2014;32(1):56–64.
21. He L, Liu Z, Liu C, Gao Z, Ren Q, Lei L, et al. Radiomics based on lumbar spine magnetic resonance imaging to detect osteoporosis. *Acad Radiol*. 2021;28(6):e165–71.
22. Hepp T, Schmid M, Gefeller O, Waldmann E, Mayr A. Approaches to regularized regression - a comparison between gradient boosting and the lasso. *Methods Inf Med*. 2016;55(5):422–30.
23. Velazquez ER, Parmar C, Jermoumi M, Mak RH, van Baardwijk A, Fennessy FM, et al. Volumetric CT-based segmentation of NSCLC using 3D-Slicer. *Sci Rep*. 2013;3:3529.
24. Rastegar S, Vaziri M, Qasempour Y, Akhsh MR, Abdalvand N, Shiri I, et al. Radiomics for classification of bone mineral loss: a machine learning study. *Diagn Interv Imaging*. 2020. <https://doi.org/10.1016/j.diii.2020.01.008>.
25. Lee KS, Jung SK, Ryu JJ, Shin SW, Choi J. Evaluation of transfer learning with deep convolutional neural networks for screening osteoporosis in dental panoramic radiographs. *J Clin Med*. 2020;9(2):392.
26. Hayashi T, Chen H, Miyamoto K, Zhou X, Hara T, Yokoyama R, et al. Analysis of bone mineral density distribution at trabecular bones in thoracic and lumbar vertebrae using X-ray CT images. *J Bone Miner Metab*. 2011;29(2):174–85.
27. Kennedy OD, Brennan O, Mahony NJ, Rackard SM, O'Brien FJ, Taylor D, Lee CT. Effects of high bone turnover on the biomechanical properties of the L3 vertebra in an ovine model of early stage osteoporosis. *Spine (Phila Pa 1976)*. 2008;33(23):2518–23. <https://doi.org/10.1097/BRS.0b013e318186b292>.
28. Samelson EJ, Christiansen BA, Demissie S, Broe KE, Louie-Gao Q, Cupples LA, et al. QCT measures of bone strength at the thoracic and lumbar spine: the Framingham Study. *J Bone Miner Res*. 2012;27(3):654–63.
29. Mao SS, Li D, Syed YS, Gao Y, Luo Y, Flores F, et al. Thoracic quantitative computed tomography (QCT) can sensitively monitor bone mineral metabolism: comparison of thoracic QCT vs lumbar QCT and dual-energy X-ray absorptiometry in detection of age-relative change in bone mineral density. *Acad Radiol*. 2017;24(12):1582–7.
30. Dickerson CR, Saha S, Hotchkiss CE. Relationships between densitometric and morphological parameters as measured by peripheral computed tomography and the compressive behavior of lumbar vertebral bodies from macaques (*Macaca fascicularis*). *Spine (Phila Pa 1976)*. 2008;33(4):366–72.
31. Yamamoto N, Sukegawa S, Kitamura A, Goto R, Noda T, Nakano K, et al. Deep learning for osteoporosis classification using hip radiographs and patient clinical covariates. *Biomolecules*. 2020;10(11):1534.
32. Shim JG, Kim DW, Ryu KH, Cho EA, Ahn JH, Kim JJ, et al. Application of machine learning approaches for osteoporosis risk prediction in postmenopausal women. *Arch Osteoporos*. 2020;15(1):169.
33. Liu J, Wang J, Ruan W, Lin C, Chen D. Diagnostic and gradation model of osteoporosis based on improved deep U-Net network. *J Med Syst*. 2019;44(1):15.
34. Huynh E, Coroller TP, Narayan V, Agrawal V, Hou Y, Romano J, et al. CT-based radiomic analysis of stereotactic body radiation therapy patients with lung cancer. *Radiother Oncol*. 2016;120(2):258–66.
35. Choe J, Lee SM, Do KH, Lee G, Lee JG, Lee SM, et al. Deep learning-based image conversion of CT reconstruction kernels improves radiomics reproducibility for pulmonary nodules or masses. *Radiology*. 2019;292(2):365–73.
36. Xue Z, Huo J, Sun X, Sun X, Ai ST, LichiZhang, et al. Using radiomic features of lumbar spine CT images to differentiate osteoporosis from normal bone density. *BMC Musculoskelet Disord*. 2022;23(1):336.
37. Burian E, Subburaj K, Mookiah MRK, Rohrmeier A, Hedderich DM, Dieckmeyer M, et al. Texture analysis of vertebral bone marrow using chemical shift encoding-based water-fat MRI: a feasibility study. *Osteoporos Int*. 2019;30(6):1265–74.
38. Nardone V, Tini P, Croci S, Carbone SF, Sebaste L, Carfagno T, et al. 3D bone texture analysis as a potential predictor of radiation-induced insufficiency fractures. *Quant Imaging Med Surg*. 2018;8(1):14–24.
39. Kim BS, Kim SJ. Prognostic value of intratumoral heterogeneity of preoperative (18) F-FDG PET/CT in pancreatic cancer. *Hell J Nucl Med*. 2021;24(3):172–7.
40. Kuyumcu ME, Yesil Y, Ozturk ZA, Cinar E, Kizilarslanoglu C, Halil M, et al. The association between homocysteine (hcy) and serum natural antioxidants in elderly bone mineral densitometry (BMD). *Arch Gerontol Geriatr*. 2012;55(3):739–43.
41. Exton-Smith AN, Carlton-Ashton JR. Neurological and mental disturbances in the elderly. Proceedings of a conference held December 1977 in Jersey, Channel Islands. *Age Ageing*. 1978;Suppl:1–140.
42. Hamed SA, Moussa EM, Youssef AH, Abd ElHameed MA, NasrEldin E. Bone status in patients with epilepsy: relationship to markers of bone remodeling. *Front Neurol*. 2014;5:142.
43. Erjiang E, Wang T, Yang L, Dempsey M, Brennan A, Ming Y, et al. Machine learning can improve clinical detection of low BMD: the DXA-HIP study. *J Clin Densitom*. 2021;24(4):527–37. <https://doi.org/10.1016/j.jocd.2020.10.004>.
44. Kilic N, Hosgormez E. Automatic estimation of osteoporotic fracture cases by using ensemble learning approaches. *J Med Syst*. 2016;40(3):61.

Publisher's Note

Springer Nature remains neutral with regard to jurisdictional claims in published maps and institutional affiliations.

Ready to submit your research? Choose BMC and benefit from:

- fast, convenient online submission
- thorough peer review by experienced researchers in your field
- rapid publication on acceptance
- support for research data, including large and complex data types
- gold Open Access which fosters wider collaboration and increased citations
- maximum visibility for your research: over 100M website views per year

At BMC, research is always in progress.

Learn more biomedcentral.com/submissions

